Lactose-Modified Chitosan Gold(III)-PEGylated Complex-Bioconjugates: From Synthesis to Interaction with Targeted Galectin-1 Protein

Qiqian Liu,[†,#] Pasquale Sacco,[∥,#] Eleonora Marsich,[⊥] Franco Furlani,[∥] Celia Arib,[†] Nadia Djaker,[†] Marc Lamy de la Chapelle,[‡,§] Ivan Donati,[∥] and Jolanda Spadavecchia*[,†]

[†]CNRS, UMR 7244, CSPBAT, Laboratoire de Chimie, Structures et Propriétés de Biomateriaux et d'Agents Therapeutiques, Université Paris 13, Sorbonne Paris Cité, 93000 Bobigny, France

[‡]Institut des Molécules et Matériaux du Mans (IMMM - UMR CNRS 6283), Le Mans Université, Avenue Olivier Messiaen, 72085 Le Mans cedex 9, France

[§]Department of Clinical Laboratory Medicine, Southwest Hospital, Third Military Medical University, 400038 Chongqing, China

[∥]Department of Life Sciences, University of Trieste, Via L. Giorgieri 5, I-34127 Trieste, Italy

[⊥]Department of Medicine, Surgery and Health Sciences, University of Trieste, Piazza dell'Ospitale 1, I-34129 Trieste, Italy

Supporting Information

ABSTRACT: Galectins (Gal) are a family of glycan-binding proteins characterized by their affinity for β-galactosides. Galectin-1 (Gal-1), a dimeric lectin with two galactoside-binding sites, regulates cancer progression and immune responses. Coordination chemistry has been engaged to develop versatile multivalent neoglycoconjugates for binding Gal-1. In this study we report a fast and original method to synthesize hybrid gold nanoparticles in which a hydrochloride lactose-modified chitosan, named CTL, is mixed with dicarboxylic acid-terminated polyethylene glycol (PEG), leading to shell-like hybrid polymer-sugar-metal nanoparticles (CTL-PEG-AuNPs). The aim of this paper is to preliminarily study the interaction of the CTL-PEG-AuNPs with a target protein, namely, Gal-1, under specific conditions. The molecular interaction has been measured by Transmission Electron Microscopy (TEM), UV−vis, and Raman Spectroscopy on a large range of Gal-1 concentrations (from 0 to 10^{-12} M). We observed that the interaction was strongly dependent on the Gal-1 concentration at the surface of the gold nanoparticles.

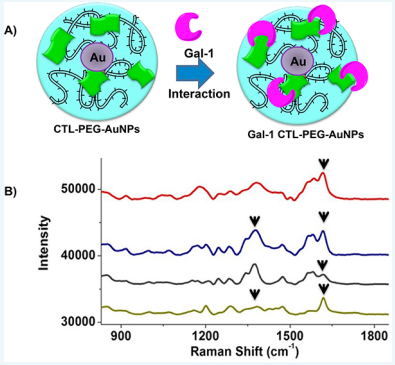

INTRODUCTION

Gold nanoparticles (AuNPs) are used in various fields as medical nanovectors, transducers, or nanosensors.[1] The research on new synthesis methods is still an active field in order to optimize the AuNPs properties for such applications.[2−4] In a previous study we have investigated a fast synthesis method to realize polymer-modified AuNPs using dycarboxylic PEG, collagen, or bisphosphonate (BPO) as stabilizers in order to demonstrate high stability and efficacy under realistic biomedical conditions.[5−8] Other authors have synthesized hybrid metal nanoparticles based on chitosan and chitosan-derivatives as sugar stabilizers for various applications in the field of the nanomedicine.[9−13]

Lactose-modified chitosan, CTL (in other papers termed Chitlac), is a branched polysaccharide synthesized via reductive *N*-alkylation of primary amines by lactose moieties (Figure S1 in Supporting Information).[14] CTL is a ternary heteropolysaccharide composed of β-1 → 4 linked glucosamine (D unit), *N*-acetyl-glucosamine (A unit), and *N*-Lactit-1-yl glucosamine (L unit) sugars. The presence of lactose residues grafted on the chitosan backbone ensures some advantages with respect to the original polymer, such as a higher solubility at neutral pH than most of commercial chitosans, miscibility with polyanions to form soluble complexes without associative phase separation, and the possibility to form gels upon mixing with boric acid as cross-linker under physiological conditions of pH and osmolarity.[15] From the biological point of view, it has been proven that CTL fosters the aggregation of an osteoblast-like cell line *in vitro*, stimulates the cell proliferation, and enhances the alkaline phosphatase activity.[16] Contextually, the aggregation of chondrocytes and the stimulation of collagen and glycosaminoglycans production was also demonstrated.[17,18] It was found that the bioactivity of CTL is ascribed to the specific interaction between the lactitol groups of the polymer and the β-galactoside-binding protein Galectin-1.[19,20]

Galectin-1 (Gal-1) is a protein differentially expressed in various normal and pathologic tissues and displays a wide

Scheme 1. Representation of the Synthesis of CTL-PEG-AuNPs[a]

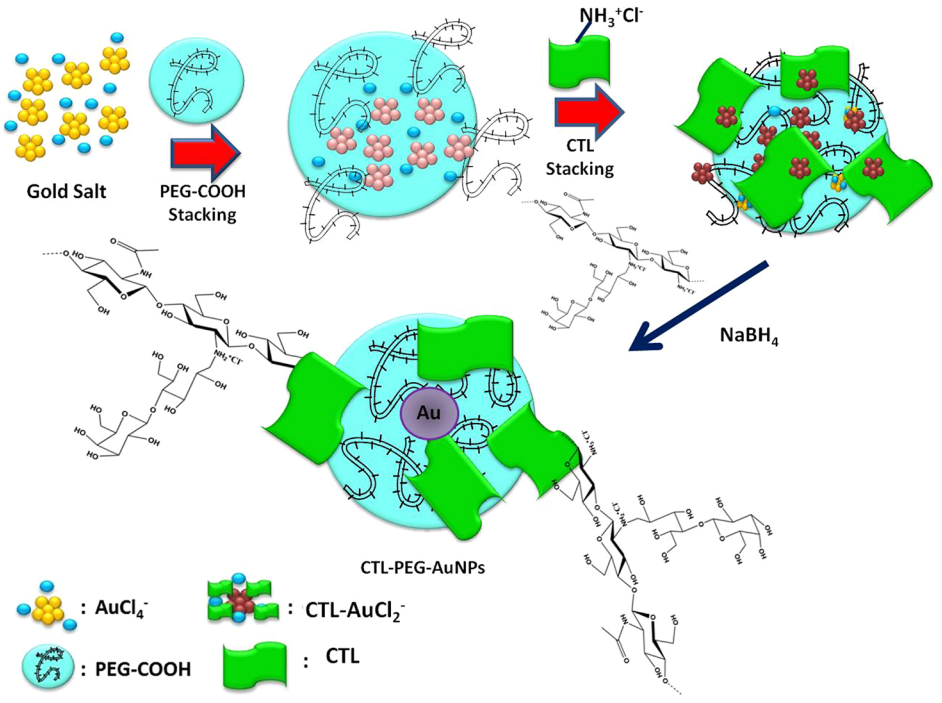

[a]Please note that drawings are not in scale and are not intended to be representative of the full sample composition.

range of activities in biological processes. Increased Gal-1 expression has been reported in different tumors such as colon, breast, lung, head and neck, ovarian, prostate carcinomas, and Hodgkin's lymphoma.[21−27] The expression of this protein in various cancer cells appears to affect tumor progression steps, mainly angiogenesis, apoptosis, cell migration, and metastatic spread. It has been recently demonstrated that Gal-1 overexpression positively correlates to tumor aggressiveness, poor patient survival, and prognosis.[28] Several studies identify this lectin as a promising therapeutic and prognostic marker in cancer.[29] Topologically, Gal-1 represents a particularly interesting challenge for targeting with synthetic, multivalent ligands[30] since it is a rigid dimer[31] with two binding sites oriented in opposite directions. The positions of the binding sites compete with each other at linear distance up to 6 nm. Since the main biological targets of Gal-1 reside on the cell surface, one strategy for targeting Gal-1 is to use structures that mimic the fluidity and adaptability of cellular membranes. Detecting and identifying this protein in biological media can then be of primary importance. However, its specific recognition needs the interaction with a bioreceptor providing a high affinity with Gal-1. The bioreceptor must be grafted at the surface of sensing transducer that could induce a modification of its affinity with the analyte to be detected. Most of the methods used to detect biomolecules require strict molecular recognition events.[32] In these latter cases, grafted biomolecules at the AuNP surface can act as bioreceptors having a high affinity for the targeted analytes.[33] The analyte target detection depends on the affinity constant of the bioreceptor to the targeted analyte.[34] The goal of the present paper is to preliminarily investigate the possibility of exploiting the interaction between CTL and Gal-1 for the development of a nanocarrier system based on CTL-decorated AuNPs for the detection and the tracking of the lectin protein.

We would like to understand whether the grafting will modify the interaction and thus if some parameters can be optimized in order to improve this interaction in terms of sensing purposes. The specific binding affinity between CTL and Gal-1 was ascertained and quantified by means of Surface Plasmon Resonance. Shell-like hybrid CTL-PEG-gold nanoparticles (CTL-PEG-AuNPs) were synthesized and characterized. The interaction between Gal-1 and CTL-PEG-AuNPs was then investigated using Localized Surface Plasmon (LSP), Transmission Electron Microscopy (TEM), and Raman spectroscopy as analytical tools.

RESULTS AND DISCUSSION

CTL-Galectin 1 Binding Affinity. In a previous paper,[1] we looked experimentally for the existence of the interaction between the polymer CTL and the lectin Gal-1 able to induce specific biological responses.

Herein, the Surface Plasmon Resonance (SPR) technique was exploited to demonstrate *in vitro* the presence of a molecular interaction between Gal-1 and CTL, and the equilibrium binding constants were calculated. To this aim CTL was immobilized on the chip via amidation chemistry. SPR signals were recorded using different concentrations of Gal-1 and corrected for the contribution of the solvent as shown in Figure S3 in Supporting Information. SPR analysis performed on nonderived polysaccharide (chitosan) allows a clear deduction that the specific interaction exists only in the case of CTL (data not shown). Interestingly, for CTL the SPR signal for concentrations of Gal-1 equal to or greater than 1 μM does not seem to reach a constant value, indicative of the achievement of a steady state. On the contrary, in the time interval in which the plateau would be expected, the signal increases linearly with slopes increasing with Gal-1 concentrations.

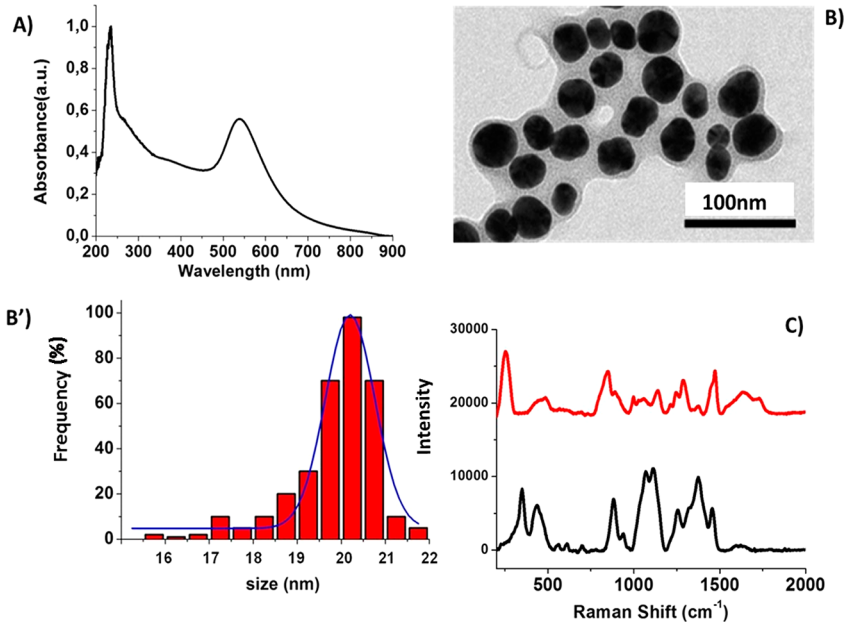

Figure 1. (A) Normalized UV−vis absorption spectrum of CTL-PEG-AuNPs, (B) TEM images of CTL-PEG-AuNPs, and size distribution histogram (B′). (C) Raman spectrum of CTL-PEG-AuNPs (red line) compared to free CTL spectrum as control (black line). (B) Scale bar: 100 nm. (C) Raman spectra. Experimental conditions: λ_{exc} = 785 nm; laser power 20 mW; accumulation time 180 s.

The analysis of the kinetic data (see Supporting Information) was carried out by adopting a model unimolecular (1:1) for the protein−substrate system providing the values of the kinetic association constant ($k_a = 6 \times 10^3$ M^{-1} s^{-1}) and kinetic dissociation constant ($k_d = 6 \times 10^{-2}$ s^{-1}) of the complex. The calculated affinity constant, defined as $K_A = k_a/k_d$, was 1×10^5 M^{-1}. The affinity constant was also calculated independently using the steady state values of the temporal trace at the different protein concentrations. The value of K_A obtained from the kinetic data was comparable with those obtained from the responses to equilibrium: 1×10^5 M^{-1} in the first case and 4×10^5 M^{-1} in the second one.

Gal-1 binds relatively strongly to CTL, in fact the calculated affinity constant (1×10^5 M^{-1}) is stronger than that reported in literature by Miller et al. for the binding of Gal-1 with the disaccharide lactose (Gal-β(1 → 4)-Glc).[36] The multivalent structure of CTL may contribute to this high analogy for Gal-1, something that is viewed with many cell-surface glycoconjugates that bear multiple galectin-binding sites.[37,38] Moreover this value is in the same range of values reported for the affinity constants for binding to both linear and complex branched glycans bearing terminal β(1 → 4)-linked galactose side chains.[39]

Formation Mechanism of CTL-PEG-AuNPs. In the past years Spadavecchia et al. have extensively investigated the synthesis of hybrid nanoparticles and the effect of various surfactant agents on the growth process.[5,6] Recently, Furlani-Sacco et al. have developed colloidal coacervates using the bioactive chitosan-derivative CTL by ionotropic gelation.[11] Contextually, other authors have designed a nanocomposite hydrogel based on natural polysaccharides, CTL, and gold nanoparticles with considerable antimicrobial activity.[20]

After demonstrating the existence of a high binding affinity between CTL and Gal-1, the objective of this paper was to evaluate the interaction between Gal-1 and CTL under formation of stable complexes of PEGylated Au (III)-CTL as active excipients of gold nanoparticles. The major discrepancy with other chemical procedures is that PEG and CTL participate in the stabilization of AuNPs via complexation between their ketone and amino groups with chloride auric ions. In our case, the formation of gold NPs from $AuCl_4^-$ comprises the following steps (Scheme 1):

1. Complexation of PEG with $AuCl_4^-$ and initial reduction of the polymer−metal complex to generate gold clusters.[7]
2. Stacking process of CTL by electrostatic adsorption onto the PEGylayed gold clusters.
3. Final reduction of metal ions at the vicinity of the clusters, growth of AuNPs and colloidal stabilization through the dicarboxylic PEG and CTL polymers.

In the first step, PEG dicarboxylic acid (PEG) is added into $HAuCl_4$ aqueous solution, to complex with it as previously described.[6,7] In the second step, the positively amino charged ($-NH_3^+$ and $-NRH_2^+$) groups of CTL in water solution favor strong electrostatic interactions with the negatively charged complex PEG-$AuCl_4^-$, the latter playing a strategic role in the growth process of AuNPs.[6] The addition of CTL in the PEG-$AuCl_4^-$ solution increases the kinetics of reduction by a further complexation with the Au ions.[6] Such an effect controls the simultaneous chemical and steric arrangement of CTL and PEG between $AuCl_4^-$ on the surface of gold seeds during the growth process of nanoparticles. In the third step, the reduction by $NaBH_4$ induces the growth process of hybrid nanoparticles.

All products were entirely characterized by UV−vis absorption spectroscopy, TEM, and Raman spectroscopy. The UV−visible spectrum of CTL-PEG-AuNPs was characterized by a surface plasmon band at 530 nm and a peak at 234 nm assigned to the CTL-PEG absorption (Figure 1A; Figure S4 in Supporting Information), which confirms the formation of AuNPs. In addition, the bright violet-blue color of the resulting nanoparticles and the UV−vis spectra remained unaltered after six months at room temperature validating the realization of stable colloidal solution.

Scheme 2. Schematic Representation of Interaction Mechanism of Galectin-1 onto CTL-PEG-AuNPs (A) and Subsequent Conformational Change of Galectin Molecules under Specific Concentrations of Protein (B)[a]

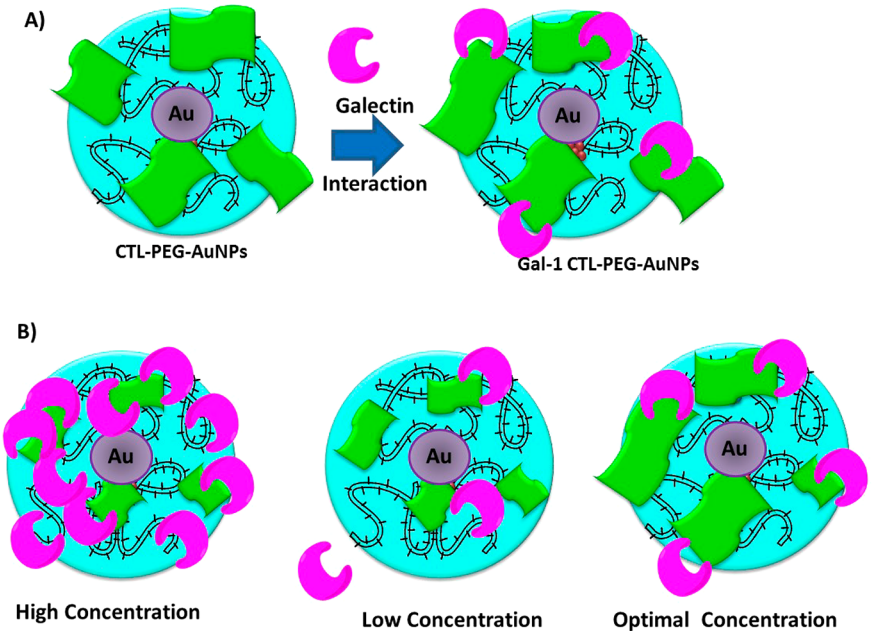

[a]Please note that drawings are not to scale and are not intended to be representative of the full samples composition.

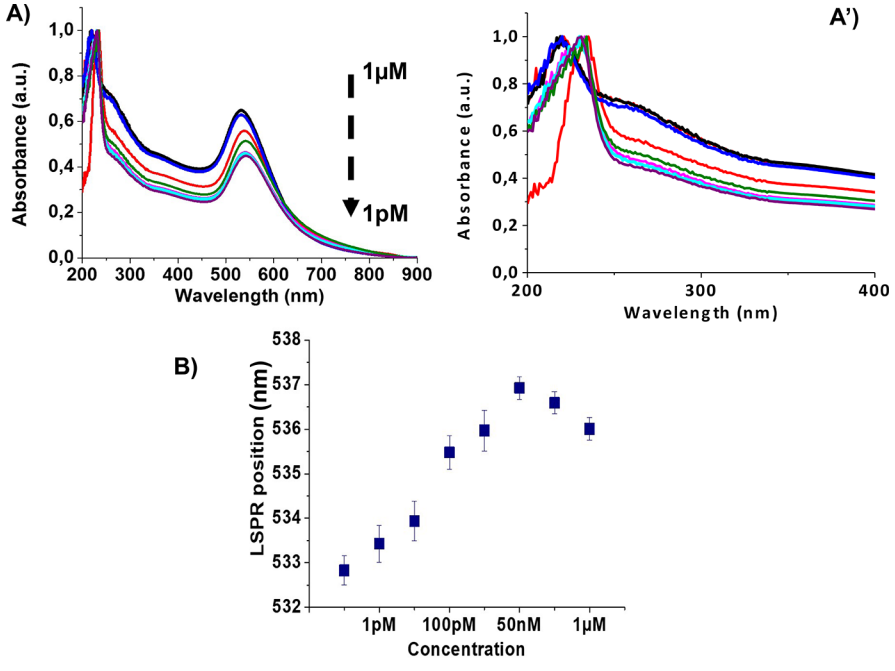

Figure 2. (A) UV−vis absorption spectra in the range 200−900 nm of CTL-PEG-AuNPs before (black line) and after (red line) interaction of Galectin-1 (from 1 μM to 1 pM) under straight condition (NaCl 0.9%). (A′) Enlargement of UV−vis absorption spectra in the range 200−400 nm of CTL-PEG-AuNPs before and after interaction of Galectin-1. (B) Evolution of the CTL-PEG-AuNPs plasmonic bands versus the Gal-1 concentration.

Representative TEM images of the colloidal solutions are shown in Figure 1 panel B. CTL-PEG-AuNPs exhibit a thin distribution in size and shape, with an average size of 20 ± 0.5 nm as estimated from 450 particles on a given TEM image. Anyway, some of the particles showed a somewhat faceted shape as a result of their nanocrystalline nature. Spadavecchia et al. have studied the synthesis of analogous nanomaterials using dicarboxylic PEG[5,6,8,35,40] obtaining PEG-AuNPs with a smaller size, i.e., about 6.7 ± 0.5 nm.[8] On the basis of previous studies[8,35,40] we assumed that, when CTL was added to the complex with the PEG-$AuCl_4^-$, the chemical and steric arrangement between PEG and CTL influences the final size of the nanoparticles.

The Raman spectra of free CTL and CTL-PEG-AuNPs in water exhibit many bands in the region 500−2000 cm^{-1} (Figure 1C). The wide band observed around 1600 cm^{-1} on

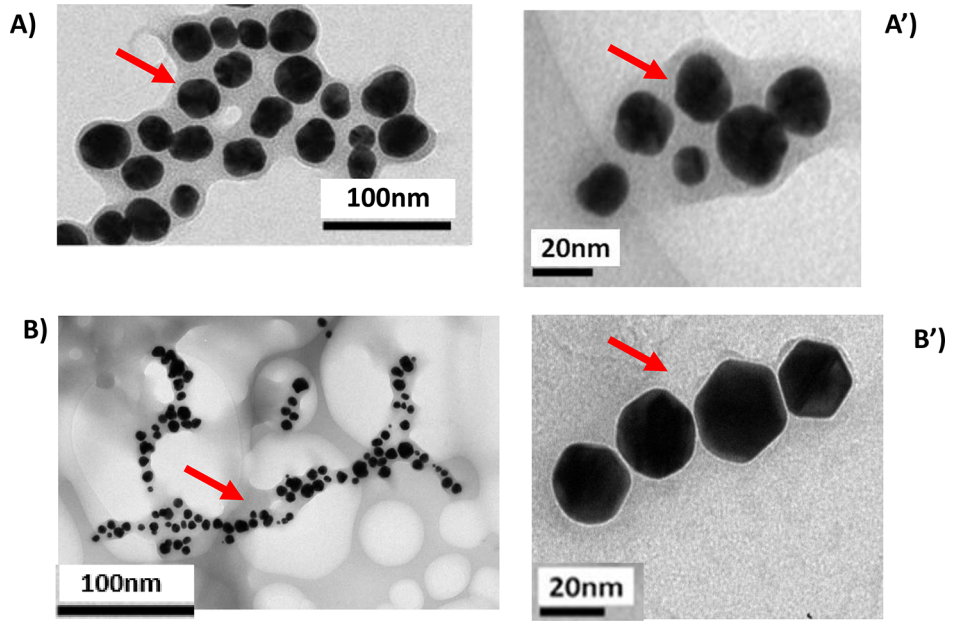

Figure 3. TEM images of CTL-PEG-AuNPs before (A,A′) and after interaction with Galectin-1 (B,B′). Scale bars: 100 nm; 20 nm (low A,B and high B,B′ magnification). Directional arrows showing a metal core of around 20 nm and suggesting the presence of an organic CTL-PEG layer of few nanometers.

the CTL-PEG-AuNPs of Raman spectra is assigned to the water. One of the Raman fingerprints of the CTL-PEG-AuNPs is the presence of a band around 263 cm^{-1} and disappearance of a double peak at 446−485 cm^{-1}. These bands can be assigned to the gold chloride stretches, ν (Au−Cl) and δ (OAuO) in aliphatic chains, and is clear evidence of the formation of a complex between $AuCl_2^-$, PEG and CTL in solution. The common peak at 430 cm^{-1} is due to the vibrations δ (OH···O), ν (OH···O) of the PEG. Based on the spectrochemical and previously theoretical results, we assumed that Au^{3+} ions promoted the deprotonation of the PEG.[35] The spectra of PEG molecules free as control were previously described in the literature[35,8] (Figure S1-A in Supporting Information). Only a few bands remain as the two bands around 1000 cm^{-1} and the one around 1620 cm^{-1}. The other ones are less intense or have completely disappeared. For instance, the strong band at 1375 cm^{-1} assigned to C═O carbonyl stretching of CTL disappears after formation of gold nanoparticles. A double peak at 1065−111 cm^{-1} due to C−O−C stretching in backbone of CTL disappears after PEG stacking onto gold nanoparticles. Furthermore, new bands also appear as an intense triplet at 1211−1243−1289 cm^{-1} due to C−O plane deformation of carboxylic acid and a strong peak at 1471 cm^{-1} assigned to ν C−C stretching. These bands are due to the variation of the steric conformation of the polymers and become more prominent upon complexation, as described previously.[35,40]

Galectin Active Interaction. Galectins are a family of glycan-binding proteins qualified by their affinity for β-galactosides and the presence of typical carbohydrate recognition domains (CRDs).[41] Several studies have shown that the linker's role, responsible for the intramolecular interactions of CRDs, is associated with the ability to induce a specific biological response.[42] For these reasons, galectins are hopeful candidates as diagnostic markers and novel drug targets for human diseases.[43−45]

CTL-PEG-AuNPs were used as building blocks to observe the biomolecular interaction with Galectin-1 (Gal-1) as protein that plays a key role in some biological processes. In order to achieve the mechanism of interaction between Gal-1 and CTL-PEG-AuNPs, Gal-1 proteins were incubated at different concentrations in the AuNPs solutions (Scheme 2). Gal-1 interacts through high binding affinity with CTL as showed by SPR measurements. The protein interaction with CTL-PEG-AuNPs was evaluated by UV−visible absorption (Figure 2). As a matter of fact, the extinction spectrum of the AuNPs is characterized by the plasmon resonance that is strongly dependent on the AuNPs environment, especially to any modification of the local dielectric constant. As a consequence, when Gal-1 interacts with CTL-PEG-AuNPs, it will modify the local environment, thus inducing a shift of the plasmon band. When Gal-1 was added to CTL-PEG-AuNPs in the range from 1 μM to 1 pM, we observed a dynamic variation of the plasmon position and width depending on the Gal-1 amount. Lowering the concentration of protein from 1 μM to 1 pM, we observed that the plasmon band red-shifted with a decrease of its width. Therefore, we assumed that the grafting of Gal-1 onto CTL-PEG-AuNPs surface induced some agglomeration of the nanoparticles due to the interaction with Gal-1 at the gold surface. The weak red shift and the decrease of the plasmon band can then be explained by a lower nanoparticle aggregation and a dissociation of agglomerates after the addition of Gal-1 at a concentration of 1 nM (Scheme 2). It means that from 1 μM up to 1 pM, Gal-1 interacts with the CTL-PEG-AuNPs inducing very small changes on the plasmon band (modification of the dielectric constant around the AuNPs with the addition of Gal-1 proteins and maybe few dissociations). At concentrations higher than 1 nM, a large number of Gal-1 proteins are expected to interact with the CTL-PEG-AuNPs forming a Gal-1 monolayer at the AuNPs surface. From 1 nM, the number of the Gal-1 is then large enough to prevent any interactions between the proteins on CTL-PEG-AuNPs, thus inducing the dissociation of the

nanoparticle agglomerates. Hence, at these concentrations we observed a blue shift of the peak due to the CTL-PEG layer from 234 to 217 nm (Figure 2A′) with the consequent decrease of the plasmon band. This effect can be due to the formation of a shell of proteins adsorbed onto the CTL-PEG-AuNPs that incessantly exchange with CTL at high concentration of Gal-1 in the environment. With the saturation of the surface of the AuNPs, we can suppose that it could induce a better orientation of the Gal-1 or a change of its conformation due to chemical hindrance and also due to protein conformation changes. The evolution of the CTL-PEG-AuNPs plasmonic bands versus the Gal-1 concentration is displayed in Figure 2B.

The protein interaction with CTL-PEG-AuNPs was also characterized by TEM. Such bioconjugates have a spherical shape (Figure 3A,B) with a diameter close to 20 nm. Following Gal-1 interaction onto CTL-PEG-AuNPs, we observed characteristic linear chain likely (Figure 3B,B′) objects, due to the preferential location of CTL-PEG and Gal-1 onto the particle surface.

The Gal-1 interaction was confirmed by DLS and Zeta potential measurements (Table S1 in Supporting Information). The hydrodynamic diameter of CTL-PEG-AuNPs was slightly higher (about 5 nm) than the radius determined by TEM analyses. This discrepancy should take into account the overestimation of the hydrodynamic diameter due to the surrounding water molecules. Besides, the ζ-potential measurements show that CTL-PEG-AuNPs and Gal-1 CTL-PEG-AuNPs were colloidally stable at physiological pH (ζ-potential = -29 ± 2 mV, for CTL-PEG-AuNPs and -25 ± 1 mV for Gal-1 CTL-PEG-AuNPs with a PDI equal to 0.3 ± 2).

The stability of CTL-PEG-AuNPs and Gal-1 CTL-PEG-AuNPs was verified in solution by visualizing the Localized Surface Plasmon (LSP) band at 530 nm. The analysis was carried out at pH 4 and electrolytic conditions up to 3 months. The synthesized CTL-PEG-AuNPs and Gal-1 CTL-PEG-AuNPs showed an almost negligible change in the LSP band position in the time frame investigated (Figure S2A,B in Supporting Information). The LPS band intensity was almost constant in the first 15 days of incubation, thus indicating the perfect stability of the systems. A slight (tolerable) reduction of LPS band intensity was noticed at 1 month. If the incubation is prolonged up to 3 months, a marked reduction of the absorbance was detected for both CTL-PEG AuNPs and Gal-1 CTL-PEG-AuNPs, thus suggesting that the systems were almost unstable for long storage purposes.

The successful interaction of Gal-1 onto CTL-PEG-AuNPs surface was established by Raman spectroscopy at different Gal-1 concentrations (Figure 4). The detection of the fingerprint of CTL and PEG-COOH at the AuNPs surface was demonstrated through the observation of the Raman bands at 1137 cm^{-1}, 1270 cm^{-1}, and 1455 cm^{-1} due to the vibration of C−O−H, C−O−C, and C−O chemical groups, respectively (Figure 4A,A′). After the Gal-1 binding, the amide II (1587−1620 cm^{-1}) and amide III (1200−1300 cm^{-1} regions), as well as modifications in protein local environments, confirmed the protein interaction (Figure 4A,A′). When the protein concentration decreased from 500 nM to 1 pM, the fingerprint of amide band was masked by water peak at 1600 cm^{-1} due to the ionic environment.

By evaluating the Raman results it was possible to confirm that the chemical and steric conformation of Gal-1 depend on molecule concentration that influences in turn the bioconjugation with CTL-PEG-AuNPs. In fact, the self-assembly of the Gal-1 on the CTL-PEG-AuNPs will take place due to their great packing density as well as the force repulsion between the negatively charged Gal-1.[30,46] However, the self-assembly of the Gal-1 on the CTL-PEG-AuNPs from 1 μM to 1 nM shows amide bands; in the presence of lower Gal-1 concentrations (from 1 μM to 1 pM) amide bands progressively disappear. This phenomenon is probably due to the swelling of polymers in water that interferes with protein steric conformation at low concentration. Similar analyses of Gal-1 interaction (UV−vis and Raman) (Figure S5 in Supporting Information) were carried out in the presence of PEG-AuNPs as control, under the same experimental conditions, confirming the selectivity of interaction between CTL-PEG-AuNPs and Gal-1. In fact, after incubating PEG-AuNPs and Gal-1 at maximal concentration (1 μM), we did not observe any signal variation.

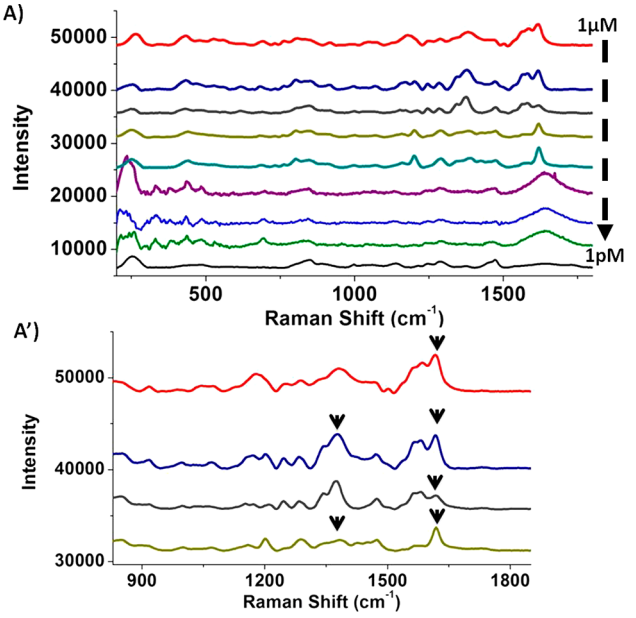

Figure 4. (A) Raman spectra of the CTL-PEG-AuNPs (red line) and Gal-1 CTL-PEG-AuNPs (Galectin-1 concentration range 1 μM − 1 pM) compared to free CTL (black line). (A′) Zoom Raman spectra of Gal-1 CTL-PEG-AuNPs from 1 μM to 500 nM; directional arrows show the characteristic peaks during protein interaction. Experimental conditions: λ_{exc} = 785 nm; laser power 20 mW; accumulation time 180 s.

Selectivity of Galectin versus CTL-PEG-AuNPs. To confirm the selectivity of Gal-1 versus CTL, a preliminary test in the presence of collagen type I was carried out. Collagen (Col) is one of several structural proteins in the extracellular matrix (ECM) overexpressed in many type of cancer. For this purpose it has been entirely used in biomedical and biomaterial applications.[47] Col solution and Col/Gal-1 mixture solution were incubated at room temperature with CTL-PEG-AuNPs at 1 μM for 18 h, and the interaction was monitored by UV−vis and Raman spectroscopy.

Figure 5A shows a shift of the plasmon position from 530 nm before interaction (black line) to 539 nm after the binding (red line) with the Col/Gal-1 mixture. A weakly widened peak at 640 nm is probably due to agglomeration between gold particles after the capture of the protein at the particle surface due to modification of the surface charges.

The protein interaction was confirmed by Raman spectroscopy. After the Col-Gal-1 interaction onto CTL-PEG-AuNPs,

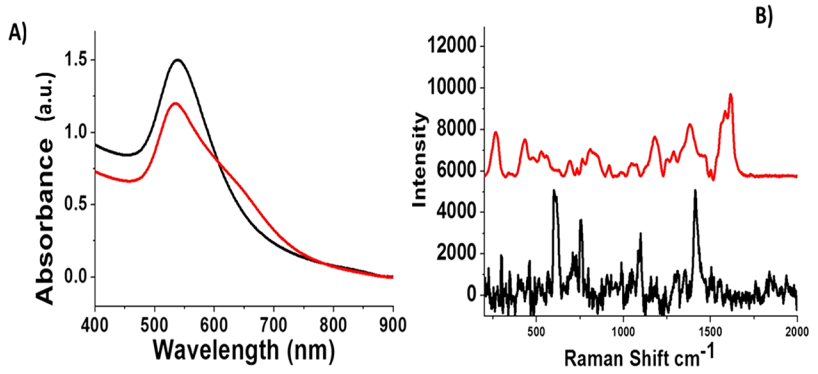

Figure 5. (A) Normalized UV−vis absorption spectrum of CTL-PEG-AuNPs before (black line) and after (red line) incubation with a mixture of Collagen (I) and Gal-1 at 1 μM. (B) Raman spectrum of CTL-PEG-AuNPs (red line) after interaction with a mixture of Collagen (I) and Gal-1 at 1 μM, compared to free CTL-PEG-AuNPs spectrum as control (black line). Raman spectra experimental conditions: λ_{exc} = 785 nm; laser power 20 mW; accumulation time 180 s.

the Raman spectrum is perfectly equivalent to Raman spectra related to single Gal-1 interaction onto CTL-PEG-AuNPs. Indeed the amide II (1587−1620 cm^{-1}) and amide III (1200−1300 cm^{-1} regions), confirmed that the Gal-1 protein is effectively captured at the AuNPs surface (Figure 5B). Moreover, the spectroscopical fingerprint of collagen is not observable. In order to assume the success of this analysis, we checked the interaction of Col *free* onto CTL-PEG-AuNPs as control (Figure S6A,B in Supporting Information), under the same experimental conditions. Figure S6 shows that, when Col was added to CTL-PEG-AuNPs, a negligible blue shift was observed in UV−vis spectra at 1 pM probably due to the chemical exchange between Col and PEG onto AuNPs surface (Figure S6A red line). However, at 1 μM, we noticed a decreased and widened peak, with a strong red shift at 680 nm due to the aggregation of AuNPs. The comparative Raman spectra at 1 pM (red line) and 1 μM (blue line) (Figure S6B Supporting Information) did not show any remarkable spectroscopical modification. This means that there was no capture of the Col at the AuNPs surface even at high concentration of Col. We thus can conclude that the CTL-PEG-AuNPs surface selectively interacts with the Gal-1.

CONCLUSIONS

In this paper, we studied for the first time the biointeraction between Galectin-1 and CTL-PEGylated gold nanoparticles. The analysis of the UV−visible and Raman spectra allowed us to highlight the formation of agglomerates due to high binding affinity between Gal-1 and CTL onto gold nanoparticles. We observed some dissociation for specific Gal-1 concentrations giving evidence of the interaction of the protein with the CTL by SPR experiments. This paper allows a better understanding of the interaction mechanism (chemical structure modifications, kinetic interaction) and the sensing optimization since the detection sensitivity is directly related to the affinity of the bioreceptor to the analyte. Further investigations are further needed to assess the *in vitro* and *in vivo* selectivity of the present system toward different cancer models.

MATERIALS AND METHODS

Materials. Tetrachloroauric acid ($HAuCl_4$), sodium borohydride ($NaBH_4$), dicarboxylic polyethylene glycol (PEG)-600 (PEG), sodium chloride (NaCl 0.9%), phosphate-buffered solution (PBS), and collagen type I were all provided by Sigma-Aldrich at maximum purity grade. Recombinant Human Galectin-1 (Lot# 0707271-1) was purchased from PeproTech (Rocky Hill, NJ, USA). Hydrochloride CTL was kindly provided by BiopoLife S.r.l. (Trieste, Italy). The chemical composition of CTL was determined by ^{1}H NMR spectroscopy and resulted in a fraction of deacetylated units (F_D) 0.36, fraction of lactose-modified units (F_L) 0.56, and fraction of acetylated units (F_A) 0.08. The physical properties were determined by viscometry: the intrinsic viscosity, [η], of CTL was checked at 25 °C by means of a CT 1150 Schott Geräte automatic measuring apparatus and a Schott capillary viscometer. A buffer solution composed by 20 mM AcOH/AcNa, pH 4.5, and 100 mM NaCl was used as solvent.[11] The resulting [η] was 511 mL/g. The estimated viscosity average molecular weight, M_v of CTL was around 870 000.

Surface Plasmon Resonance Analysis. The interaction between CTL and Gal-1 was assessed by means of a Biacore TM 2000 Instrument (BIAcore, Uppsala, Sweden) using a Chip sensor CM5 (GE Healthcare). CTL was immobilized on the chip following manufacturer's instructions. Briefly, CTL was dissolved in AcOH/AcNa buffer, pH 4.5, at a concentration of 0.05 g/L. Subsequently, CTL was injected (30 μL/min) on the chip surface until a SPR signal of approximately 800 RU was observed.

Gal-1 solubilization and binding measurements were performed in PBS buffer, pH 7, supplemented with dithiothreitol (DTT-2 mM) and P20 detergent (0.005%). Gal-1 solutions in a range of concentrations 0.12−8 μM were injected over the sensor chip surface at 30 μL/min. Flow channel Fc1 has been used as negative control. The chip was regenerated by injection of lactose 10 mM. Data analysis has been performed by the BIA evaluation 3.2 Software (Biacore). A Langmuir 1:1 model was used for the calculation of rate constants (for details see Supporting Information).

Preparation of CTL and Galectin Protein Solutions. CTL was solubilized at a concentration equal to 1 mg/mL in Milli-Q water (final pH around 3). Galectin powder was solubilized in water and then diluted in order to obtain solutions with concentrations comprised within the range 1 μM − 1 pM. Molar concentrations of Galectin-1 were determined taking into account that the molecular weight of Galectin-1 is equal to 14.5 kDa.

Preparation of Collagen and Galectin Protein Solutions (Selectivity Test). Galectin and Collagen were solubilized in water and mixed together to obtain a solution at concentration of 1 μM.

Synthesis of CTL-PEG-AuNPs. Colloids of CTL-PEG-coated AuNPs (CTL-PEG-AuNPs) were synthesized by a well-established chemical reduction process described in Scheme 1. Briefly, 250 μL of PEG solution (0.5 mM) was added to 20 mL of tetrachloroauric acid solution (2.4×10^{-4} M) under stirring at room temperature. Then, 5 mL of CTL solution (1 mg/mL) and 2 mL of aqueous 0.01 M $NaBH_4$ were added drop by drop with precaution until solution turned into a violet color. The concentration was estimated by standard mathematical calculations in colloidal solution.

Determination of CTL-PEG-AuNPs Concentration. AuNPs concentration was determined by exploiting standard mathematical calculations in colloidal solution. Lambert−Beer law ($A = \varepsilon\ C\ l$) was used to determine colloids concentration. In this equation, A is the maximum absorbance (corresponding to the Surface Plasmon Resonance Band at around 530−540 nm) of the UV−visible spectrum, ε is the molar extinction coefficient (equal to 3.07×10^{10} M^{-1} cm^{-1}), C is the molar concentration of colloids, and l is the optical length of cuvette (1 cm). The resulting C was multiplied for the dilution factor to obtain the concentration of colloids.

Bioconjugation of CTL-PEG-AuNPs with Gal-1. The interaction of Gal-1 protein with CTL-PEG-AuNPs surface was obtained exploiting the procedures depicted in Scheme 2. Briefly, 5 mL of CTL-PEG-AuNPs (42 nM) were added into separate tubes containing 50 μL of Gal-1 (from 1 μM to 1 pM; PBS pH 7; NaCl 0.15 M). After 18 h of incubation, the CTL-PEG-AuNPs/Gal-1 suspension was centrifuged twice at 5000 rpm for 10 min to eliminate the excess of Gal-1 and then the pellets were redispersed in 1 mL of Milli-Q water as described previously.[8]

Physical-Chemical Characterization. All the measurements were accomplished in triplicate to confirm the reproducibility of the synthetic and analytical procedures.

UV/vis Measurements. Absorption spectra were recorded using a double-beam Varian Cary 500 UV−vis spectrophotometer (Agilent, France). UV−vis spectra of the AuNPs were achieved in water at concentration of 42 nM in the 200−900 nm spectral range.

Transmission Electron Microscopy (TEM). Transmission Electron Microscopy (TEM) images were recorded with a JEOL JEM 1011 microscope operating (JEOL, USA) at an accelerating voltage of 100 kV. TEM specimens were prepared after separating the surfactant from the metal particles by centrifugation under a protocol described previously.[8]

Raman Spectroscopy. The Raman experiments have been performed on an Xplora spectrometer (Horiba Scientifics-France) under a protocol described previously.[8]

Dynamic Light Scattering (DLS) and Zeta Potential Measurements. The size and zeta potential measurements were performed using a Zetasizer Nano ZS (Malvern Instruments, Malvern, UK) equipped with a He−Ne laser (633 nm, fixed scattering angle of 173°) at room temperature as described previously.[35]

Stability of CTL-PEG-AuNPs and Gal-1 CTL-PEGAuNPs as a Function of pH. The stability of nanoparticles was detected by UV−vis. All nanoparticles were dissolved in PBS buffer, NaCl 0.15 M, pH 4 and stored for 3 months (Figure S2 in Supporting Information).

■ ASSOCIATED CONTENT

● **Supporting Information:**

Supplementary figures, schemes and tables are provided (PDF)

■ AUTHOR INFORMATION

Corresponding Author

*E-mail: jolanda.spadavecchia@univ-paris13.fr.

ORCID

Pasquale Sacco: 0000-0002-4483-5099
Franco Furlani: 0000-0001-5986-1727
Nadia Djaker: 0000-0001-7912-5436
Ivan Donati: 0000-0003-3752-8346
Jolanda Spadavecchia: 0000-0001-6697-1174

Author Contributions

The manuscript was written through contributions of all authors. All authors have given approval to the final version of the manuscript.

Author Contributions

#These authors (Qiqian Lisu, Pasquale Sacco) contributed equally.

Notes

The authors declare no competing financial interest.

■ ACKNOWLEDGMENTS

This work has been partly performed on the CNanoMat platform of the University Paris 13. This study was supported by the University of Trieste (FRADONATI2016-17) and by the INTERREG V-A ITALIA-SLOVENIA 2014-2020 BANDO 1/2016 ASSE 1 - project BioApp 1472551605.

■ REFERENCES

(1) Marcon, P., Marsich, E., Vetere, A., Mozetic, P., Campa, C., Donati, I., Vittur, F., Gamini, A., and Paoletti, S. (2005) The role of Galectin-1 in the interaction between chondrocytes and a lactose-modified chitosan. *Biomaterials 26* (24), 4975−84.

(2) Sapsford, K. E., Algar, W. R., Berti, L., Gemmill, K. B., Casey, B. J., Oh, E., Stewart, M. H., and Medintz, I. L. (2013) Functionalizing Nanoparticles with Biological Molecules: Developing Chemistries that Facilitate Nanotechnology. *Chem. Rev. 113* (3), 1904−2074.

(3) Moore, T. L., Rodriguez-Lorenzo, L., Hirsch, V., Balog, S., Urban, D., Jud, C., Rothen-Rutishauser, B., Lattuada, M., and Petri-Fink, A. (2015) Nanoparticle colloidal stability in cell culture media and impact on cellular interactions. *Chem. Soc. Rev. 44* (17), 6287−6305.

(4) Jans, H., Liu, X., Austin, L., Maes, G., and Huo, Q. (2009) Dynamic Light Scattering as a Powerful Tool for Gold Nanoparticle Bioconjugation and Biomolecular Binding Studies. *Anal. Chem. 81* (22), 9425−9432.

(5) Politi, J., De Stefano, L., Longobardi, S., Giardina, P., Rea, I., Methivier, C., Pradier, C. M., Casale, S., and Spadavecchia, J. (2015) The amphiphilic hydrophobin Vmh2 plays a key role in one step synthesis of hybrid protein-gold nanoparticles. *Colloids Surf., B 136*, 214−21.

(6) Spadavecchia, J., Apchain, E., Alberic, M., Fontan, E., and Reiche, I. (2014) One-step synthesis of collagen hybrid gold nanoparticles and formation on Egyptian-like gold-plated archaeological ivory. *Angew. Chem., Int. Ed. 53* (32), 8363−6.

(7) Spadavecchia, J., Perumal, R., Barras, A., Lyskawa, J., Woisel, P., Laure, W., Pradier, C. M., Boukherroub, R., and Szunerits, S. (2014)

Amplified plasmonic detection of DNA hybridization using doxorubicin-capped gold particles. *Analyst 139* (1), 157−64.
(8) Spadavecchia, J., Movia, D., Moore, C., Maguire, C. M., Moustaoui, H., Casale, S., Volkov, Y., and Prina-Mello, A. (2016) Targeted polyethylene glycol gold nanoparticles for the treatment of pancreatic cancer: from synthesis to proof-of-concept in vitro studies. *Int. J. Nanomed. 11*, 791−822.
(9) Tammam, S. N., Khalil, M. A. F., Abdul Gawad, E., Althani, A., Zaghloul, H., and Azzazy, H. M. E. (2017) Chitosan gold nanoparticles for detection of amplified nucleic acids isolated from sputum. *Carbohydr. Polym. 164*, 57−63.
(10) Donati, I., Travan, A., Pelillo, C., Scarpa, T., Coslovi, A., Bonifacio, A., Sergo, V., and Paoletti, S. (2009) Polyol Synthesis of Silver Nanoparticles: Mechanism of Reduction by Alditol Bearing Polysaccharides. *Biomacromolecules 10* (2), 210−213.
(11) Furlani, F., Sacco, P., Marsich, E., Donati, I., and Paoletti, S. (2017) Highly monodisperse colloidal coacervates based on a bioactive lactose-modified chitosan: From synthesis to characterization. *Carbohydr. Polym. 174*, 360−368.
(12) Manivasagan, P., Bharathiraja, S., Bui, N. Q., Lim, I. G., and Oh, J. (2016) Paclitaxel-loaded chitosan oligosaccharide-stabilized gold nanoparticles as novel agents for drug delivery and photoacoustic imaging of cancer cells. *Int. J. Pharm. 511* (1), 367−379.
(13) Collado-Gonzalez, M., Montalban, M. G., Pena-Garcia, J., Perez-Sanchez, H., Villora, G., and Diaz Banos, F. G. (2017) Chitosan as stabilizing agent for negatively charged nanoparticles. *Carbohydr. Polym. 161*, 63−70.
(14) Donati, I., Stredanska, S., Silvestrini, G., Vetere, A., Marcon, P., Marsich, E., Mozetic, P., Gamini, A., Paoletti, S., and Vittur, F. (2005) The aggregation of pig articular chondrocyte and synthesis of extracellular matrix by a lactose-modified chitosan. *Biomaterials 26* (9), 987−98.
(15) (a) Marsich, E., Travan, A., Feresini, M., Lapasin, R., Paoletti, S., and Donati, I. (2013) Polysaccharide-Based Polyanion−Polycation−Polyanion Ternary Systems in the Concentrated Regime and Hydrogel Form. *Macromol. Chem. Phys. 214* (12), 1309−1320. (b) Sacco, P., Furlani, F., Cok, M., Travan, A., Borgogna, M., Marsich, E., Paoletti, S., and Donati, I. (2017) Boric Acid Induced Transient Cross-Links in Lactose-Modified Chitosan (Chitlac). *Biomacromolecules 18* (12), 4206−4213. (c) Cok, M., Sacco, P., Porrelli, D., Travan, A., Borgogna, M., Marsich, E., Paoletti, S., and Donati, I. (2018) Mimicking mechanical response of natural tissues. Strain hardening induced by transient reticulation in lactose-modified chitosan (chitlac). *Int. J. Biol. Macromol. 106*, 656−660.
(16) Travan, A., Marsich, E., Donati, I., Foulc, M.-P., Moritz, N., Aro, H. T., and Paoletti, S. (2012) Polysaccharide-Coated Thermosets for Orthopedic Applications: From Material Characterization to In Vivo Tests. *Biomacromolecules 13* (5), 1564−1572.
(17) Lei, M., Liu, S.-q., and Liu, Y.-l. (2008) Resveratrol protects bone marrow mesenchymal stem cell derived chondrocytes cultured on chitosan-gelatin scaffolds from the inhibitory effect of interleukin-1β. *Acta Pharmacol. Sin. 29*, 1350.
(18) Marsich, E., Borgogna, M., Donati, I., Mozetic, P., Strand, B. L., Salvador, S. G., Vittur, F., and Paoletti, S. (2008) Alginate/lactose-modified chitosan hydrogels: a bioactive biomaterial for chondrocyte encapsulation. *J. Biomed. Mater. Res., Part A 84* (2), 364−76.
(19) Mendoza, G., Regiel-Futyra, A., Andreu, V., Sebastián, V., Kyzioł, A., Stochel, G., and Arruebo, M. (2017) Bactericidal Effect of Gold−Chitosan Nanocomposites in Coculture Models of Pathogenic Bacteria and Human Macrophages. *ACS Appl. Mater. Interfaces 9* (21), 17693−17701.
(20) Marsich, E., Travan, A., Donati, I., Di Luca, A., Benincasa, M., Crosera, M., and Paoletti, S. (2011) Biological response of hydrogels embedding gold nanoparticles. *Colloids Surf., B 83* (2), 331−9.
(21) Barrow, H., Rhodes, J. M., and Yu, L. G. (2011) The role of galectins in colorectal cancer progression. *Int. J. Cancer 129* (1), 1−8.
(22) Dalotto-Moreno, T., Croci, D. O., Cerliani, J. P., Martinez-Allo, V. C., Dergan-Dylon, S., Méndez-Huergo, S. P., Stupirski, J. C., Mazal, D., Osinaga, E., Toscano, M. A., Sundblad, V., Rabinovich, G. A., and Salatino, M. (2013) Targeting Galectin-1 Overcomes Breast Cancer-Associated Immunosuppression and Prevents Metastatic Disease. *Cancer Res. 73* (3), 1107−1117.
(23) Szöke, T., Kayser, K., Baumhäkel, J. D., Trojan, I., Furak, J., Tiszlavicz, L., Horvath, A., Szluha, K., Gabius, H. J., and Andre, S. (2005) Prognostic Significance of Endogenous Adhesion/Growth-Regulatory Lectins in Lung Cancer. *Oncology 69* (2), 167−174.
(24) Saussez, S., Camby, I., Toubeau, G., and Kiss, R. (2007) Galectins as modulators of tumor progression in head and neck squamous cell carcinomas. *Head & Neck 29* (9), 874−884.
(25) Chow, S. N., Chen, R. J., Chen, C. H., Chang, T. C., Chen, L. C., Lee, W. J., Shen, J., and Chow, L. P. (2010) Analysis of protein profiles in human epithelial ovarian cancer tissues by proteomic technology. *Eur. J. Gynaecol Oncol 31* (1), 55−62.
(26) Laderach, D. J., Gentilini, L. D., Giribaldi, L., Delgado, V. C., Nugnes, L., Croci, D. O., Al Nakouzi, N., Sacca, P., Casas, G., Mazza, O., Shipp, M. A., Vazquez, E., Chauchereau, A., Kutok, J. L., Rodig, S. J., Elola, M. T., Compagno, D., and Rabinovich, G. A. (2013) A unique galectin signature in human prostate cancer progression suggests galectin-1 as a key target for treatment of advanced disease. *Cancer Res. 73* (1), 86−96.
(27) Gandhi, M. K., Moll, G., Smith, C., Dua, U., Lambley, E., Ramuz, O., Gill, D., Marlton, P., Seymour, J. F., and Khanna, R. (2007) Galectin-1 mediated suppression of Epstein-Barr virus−specific T-cell immunity in classic Hodgkin lymphoma. *Blood 110* (4), 1326−1329.
(28) Thijssen, V. L., Heusschen, R., Caers, J., and Griffioen, A. W. (2015) Galectin expression in cancer diagnosis and prognosis: A systematic review. *Biochim. Biophys. Acta, Rev. Cancer 2*, 235−47.
(29) Astorgues-Xerri, L., Riveiro, M. E., Tijeras-Raballand, A., Serova, M., Neuzillet, C., Albert, S., Raymond, E., and Faivre, S. (2014) Unraveling galectin-1 as a novel therapeutic target for cancer. *Cancer Treat. Rev. 40* (2), 307−19.
(30) Pieters, R. J. (2006) Inhibition and Detection of Galectins. *ChemBioChem 7* (5), 721−728.
(31) Bourne, Y., Bolgiano, B., Liao, D.-I., Strecker, G., Cantau, P., Herzberg, O., Feizi, T., and Cambillau, C. (1994) Crosslinking of mammalian lectin (galectin-1) by complex biantennary saccharides. *Nat. Struct. Mol. Biol. 1*, 863.
(32) Rajeeva, B. B., Hernandez, D. S., Wang, M., Perillo, E., Lin, L., Scarabelli, L., Pingali, B., Liz-Marzán, L. M., Dunn, A. K., Shear, J. B., and Zheng, Y. (2015) Regioselective Localization and Tracking of Biomolecules on Single Gold Nanoparticles. *Advanced Science 2* (11), 1500232.
(33) Richman, S. A., Kranz, D. M., and Stone, J. D. (2009) Biosensor detection systems: engineering stable, high-affinity bioreceptors by yeast surface display. *Methods in molecular biology (Clifton, N.J.) 504*, 323−50.
(34) Vo-Dinh, T. (2008) Nanosensing at the single cell level(). *Spectrochim. Acta, Part B 63* (2), 95−103.
(35) Moustaoui, H., Movia, D., Dupont, N., Bouchemal, N., Casale, S., Djaker, N., Savarin, P., Prina-Mello, A., de la Chapelle, M. L., and Spadavecchia, J. (2016) Tunable Design of Gold(III)-Doxorubicin Complex-PEGylated Nanocarrier. The Golden Doxorubicin for Oncological Applications. *ACS Appl. Mater. Interfaces 8* (31), 19946−57.
(36) Miller, M. C., Nesmelova, I. V., Platt, D., Klyosov, A., and Mayo, K. H. (2009) The carbohydrate-binding domain on galectin-1 is more extensive for a complex glycan than for simple saccharides: implications for galectin-glycan interactions at the cell surface. *Biochem. J. 421* (2), 211−21.
(37) Collins, B. E., and Paulson, J. C. (2004) Cell surface biology mediated by low affinity multivalent protein-glycan interactions. *Curr. Opin. Chem. Biol. 8* (6), 617−25.
(38) Bumba, L., Laaf, D., Spiwok, V., Elling, L., Kren, V., and Bojarova, P. (2018) Poly-N-Acetyllactosamine Neo-Glycoproteins as Nanomolar Ligands of Human Galectin-3: Binding Kinetics and Modeling. *Int. J. Mol. Sci. 19* (2), 372.

(39) Stowell, S. R., Arthur, C. M., Mehta, P., Slanina, K. A., Blixt, O., Leffler, H., Smith, D. F., and Cummings, R. D. (2008) Galectin-1, −2, and −3 exhibit differential recognition of sialylated glycans and blood group antigens. *J. Biol. Chem. 283* (15), 10109−23.
(40) Marguerit, G., Moustaoui, H., Haddada, M. B., Djaker, N., Chapelle, M. L., and Spadavecchia, J. (2018) Taxanes Hybrid Nanovectors: From Design to Physico-Chemical Evaluation of Docetaxel and Paclitaxel Gold (III)-PEGylated Complex Nanocarriers. *Particle & Particle Systems Characterization 35* (2), 1700299.
(41) Johannes, L., Wunder, C., and Shafaq-Zadah, M. (2016) Glycolipids and Lectins in Endocytic Uptake Processes. *J. Mol. Biol. 428*, 4792.
(42) Cousin, J. M., and Cloninger, M. J. (2016) The Role of Galectin-1 in Cancer Progression, and Synthetic Multivalent Systems for the Study of Galectin-1. *Int. J. Mol. Sci. 17* (9), 1566.
(43) Chuang, C.-H., Du, Y.-C., Wu, T.-F., Chen, C.-H., Lee, D.-H., Chen, S.-M., Huang, T.-C., Wu, H.-P., and Shaikh, M. O. (2016) Immunosensor for the ultrasensitive and quantitative detection of bladder cancer in point of care testing. *Biosens. Bioelectron. 84*, 126−132.
(44) Ebrahim, A. H., Alalawi, Z., Mirandola, L., Rakhshanda, R., Dahlbeck, S., Nguyen, D., Jenkins, M., Grizzi, F., Cobos, E., Figueroa, J. A., and Chiriva-Internati, M. (2014) Galectins in cancer: carcinogenesis, diagnosis and therapy. *Annals of Translational Medicine 2* (9), 88.
(45) Besford, Q. A., Wojnilowicz, M., Suma, T., Bertleff-Zieschang, N., Caruso, F., and Cavalieri, F. (2017) Lactosylated Glycogen Nanoparticles for Targeting Prostate Cancer Cells. *ACS Appl. Mater. Interfaces 9* (20), 16869−16879.
(46) Belitsky, J. M., Nelson, A., Hernandez, J. D., Baum, L. G., and Stoddart, J. F. (2007) Multivalent interactions between lectins and supramolecular complexes: Galectin-1 and self-assembled pseudopolyrotaxanes. *Chem. Biol. 14* (10), 1140−51.
(47) Xu, B., Chow, M.-J., and Zhang, Y. (2011) Experimental and Modeling Study of Collagen Scaffolds with the Effects of Crosslinking and Fiber Alignment. *Int. J. Biomater. 2011*, 172389.